Thermal Enhancement of Interference Effects in Quantum Point Contacts

Adel Abbout, Gabriel Lemarié, and Jean-Louis Pichard

Service de Physique de l'État Condensé (CNRS URA 2464), IRAMIS/SPEC, CEA Saclay, 91191 Gif-sur-Yvette, France

(Received 16 November 2010; revised manuscript received 22 March 2011; published 15 April 2011)

We study an electron interferometer formed with a quantum point contact and a scanning probe tip in a two-dimensional electron gas. The images giving the conductance as a function of the tip position exhibit fringes spaced by half the Fermi wavelength. For a contact opened at the edges of a quantized conductance plateau, the fringes are enhanced as the temperature T increases and can persist beyond the thermal length l_T. This unusual effect is explained by assuming a simplified model: The fringes are mainly given by a contribution which vanishes when $T \to 0$ and has a decay characterized by a T-independent scale.

DOI: 10.1103/PhysRevLett.106.156810 PACS numbers: 85.35.Ds, 07.79.−v, 72.10.−d, 73.23.−b

In mesoscopic physics, the interference effects are usually important when the temperature $T = 0$, and disappear as T increases, at scales larger than the thermal length $l_T \propto 1/T$. We show in this Letter that there are interferometers exhibiting the opposite behavior, where interference fringes are larger when $T \neq 0$ and persist beyond l_T. For instance, let us take an electron interferometer made of two scatterers, one of them having a sharp resonance such that it is transparent at the Fermi energy E_F and scatters only the electrons of energy $E \neq E_F$. In that case, Fermi-Dirac statistics give rise to a temperature-induced interferometer which disappears as $T \to 0$. Such an interferometer exhibits temperature-induced fringes (TIFs). A magnetic impurity or a quantum dot exhibiting a Kondo resonance at E_F could provide such a resonant scatterer. We consider here a simpler scatterer without many-body effects, the resonance level model (RLM), where a tunable level is put in a contact between two leads, giving rise to a resonant peak in the contact transmission. With all the current flowing through the contact, this geometry enhances the effect of the resonance and favors large TIFs. The temperature dependence of the TIFs resulting from the interferences between the resonant level and another scatterer put in the leads can be analytically given from this exactly solvable model.

Moreover, we show that TIFs characterize also electron interferometers made of a quantum point contact (QPC) and the depletion region created by the charged tip of a scanning gate microscope (SGM). Though the QPC has no true resonances, the sharp opening of its conductance channels can also give rise to TIFs, for special values of the QPC opening. This is particularly interesting, since the QPCs are used in a wide variety of investigations, including various prototypes of quantum-computing schemes. By using a two-dimensional electron gas created just beneath the surface of a semiconductor heterostructure, the QPC can be induced by electrostatic gates. The quantization [1,2] in units of $2e^2/h$ of its conductance g can be explained by using simple noninteracting models [3–5], outside some anomalies, such as the $0.7(2e^2/h)$ anomaly [6], which cannot be explained by a noninteracting theory. The recent engineering [7–10] of the SGM has allowed several experimental groups to ''image'' the electron flow associated with the successive conductance plateaus [7,9] of a QPC. The images are obtained with the charged tip of an atomic force microscope which can be scanned over the surface of the heterostructure. A negatively charged tip causes a depletion region in the two-dimensional electron gas underneath the tip which scatters the electrons at a distance r from the QPC. The tip and the QPC form an electron interferometer, and the SGM images give its conductance g as a function of the tip position. Fringes falling off with r and spaced by half the Fermi wavelength $\lambda_F/2$ characterize these images. As recently pointed [11] out, the effect of a charged tip upon g is more important if the QPC is biased between the conductance plateaus than inside the plateaus.

We show that temperature can give rise to TIFs if the QPC is biased near the ends of a plateau. Moreover, the scale characterizing the TIF decay is not l_T but another length l_Γ associated with the sharpness of the conductance steps. Fringes persisting above l_T have been seen [8] in the middle of the plateaus, and the role of impurity scattering was important for explaining this persisting fringing [12,13]. Here, we give another mechanism for fringes persisting beyond l_T, valid without impurity scattering. It takes place only at the edges of the plateaus, and its observation requires a sharp opening of the QPC conduction channels.

Numerical observations from QPC models.—Our observations are based on numerical simulations of ballistic models where the only source of scattering outside the QPC comes from the depletion region caused by the charged tip. This limit was experimentally studied in Refs. [12,14]. We neglect electron-electron interactions acting inside the QPC, though they can change the SGM images of a weakly opened contact [15]. Therefore, our results exhibit neither the branches [8] nor the $0.7(2e^2/h)$ anomaly seen in the experiments. By using lattice models with small filling factors for describing a broad infinite

strip in the continuum limit, a long adiabatic QPC characterized by a sharp opening of its conduction channels [3] is defined in a central scattering region. Model 1 consists in a smooth saddle-point contact [4], while model 2 has hard walls (see Fig. 1 and its caption). The effect of the charged tip is modeled by a potential $V \neq 0$ at a site of coordinates $(x = X - L_X, y = L_Y)$.

Typical SGM images are shown in Fig. 2 using a QPC biased at the edge of the first two conductance plateaus. At $T = 0$, the conductance without the tip g_0 is an integer [see the insets which give $g_0(E)$, the arrows indicating the value of E_F], and the interference effects are weak [Figs. 2(a) and 2(c)]. Increasing T induces TIFs, as shown in Figs. 2(b) and 2(d). When $g_0 = 1$ the TIFs are in the longitudinal X direction, while they have a V shape when $g_0 = 2$. These patterns have been observed [7] in the middle of the plateaus. A checkerboard pattern of the type discussed in Ref. [12] can be seen in Fig. 2(b). Last but not least, in Fig. 2(d), TIFs can be seen up to $r \approx 4l_T$ (the thermal length $l_T \approx 4\lambda_F/2$); thus, we have persistent fringing beyond l_T, a phenomenon observed and explained when there are other scatterers near the tip (see [8,12,13]), which is not the case here.

Though this occurrence of fringes with temperature looks extraordinary, it can be simply explained. For a QPC of reflection and transmission amplitudes $x_{\rm qpc}$ and $t_{\rm qpc}$, let us consider the paths sketched in Fig. 1(a) which contribute to the total reflection R: the path A (QPC reflection) and the path B (tip reflection), of respective amplitudes $a \propto x_{\rm qpc}$ and $b \propto t_{\rm qpc}^2 (V/x) \exp(2ik_F x)$. On the first plateau, $x_{\rm qpc} = 0$ at E_F and the effect of the tip falls off as

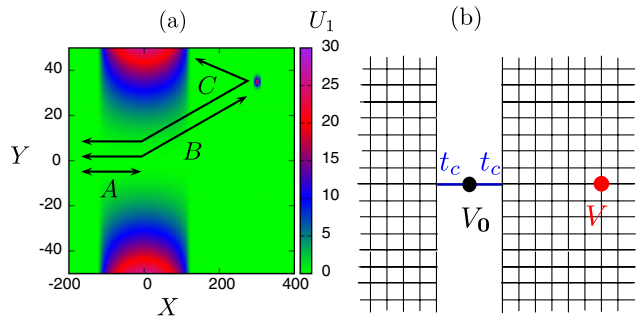

FIG. 1 (color online). Electron interferometer made of a QPC and a scatterer (red point on the right) induced by a charged tip. The lines with two arrowheads give the main interference paths responsible for the SGM fringes. (a) Saddle-point QPC potential used in model 1: $U_1(X, Y) = (Y/L_Y)^2[1 - 3(X/L_X)^2 + 2|X/L_X|^3]^{1/4}$ for $|X| \leq L_X$ and $U_1 = 0$ elsewhere. $L_Y = 10$ and $L_X = 120$ (i.e., long QPC). Model 2 (hard wall QPC not shown) consists in removing for $|X| \leq L_X$ the sites of coordinates $|Y| \geq L_Y + 3(X/L_X)^2$, with $L_Y = 6$ and $L_X = 20$ but keeping otherwise the site potentials equal to zero. The hopping amplitudes are $t_h = -1$. (b) RLM: 2 semi-infinite square lattices (with zero on-site potential and hopping amplitudes $t_h = -1$) are contacted by hopping terms t_c via a single site **0** of energy V_0. At a distance x from the contact, there is a tip potential $V \neq 0$.

$|b|^2 \propto (V/x)^2$ at $T = 0$. The fringes come from the interferences of path B with longer paths C, giving a checkerboard pattern [12]. When $T \neq 0$, the electron beam contributing to transport acquires a width $k_B T$. If E_F is located at the edge of the first plateau at $T = 0$ [arrow in Fig. 2(a)], electrons of energies below E_F for which $x_{\rm qpc} \neq 0$ begin to contribute to g, and interferences between paths A and B give a contribution $\approx |a + b|^2 \propto V/x$ of period $\lambda_F/2$ to R. This explains the TIFs observed when $T \neq 0$.

Analytical solution of a RLM.—For quantitatively describing the TIFs, we study the interferometer sketched in Fig. 1(b): two leads contacted via a *single* site **0** of energy $V_{\mathbf{0}}$ and coordinates (0, 0) with hopping terms t_c. The effect of the tip is modeled by a potential $V \neq 0$ at the site $(x, 0)$ in the right lead. While for a QPC the conductance without tip $g_0(E)$ is a steplike function and $g_0 = 1$ inside the first plateau, for the RLM model it is a Lorentzian with

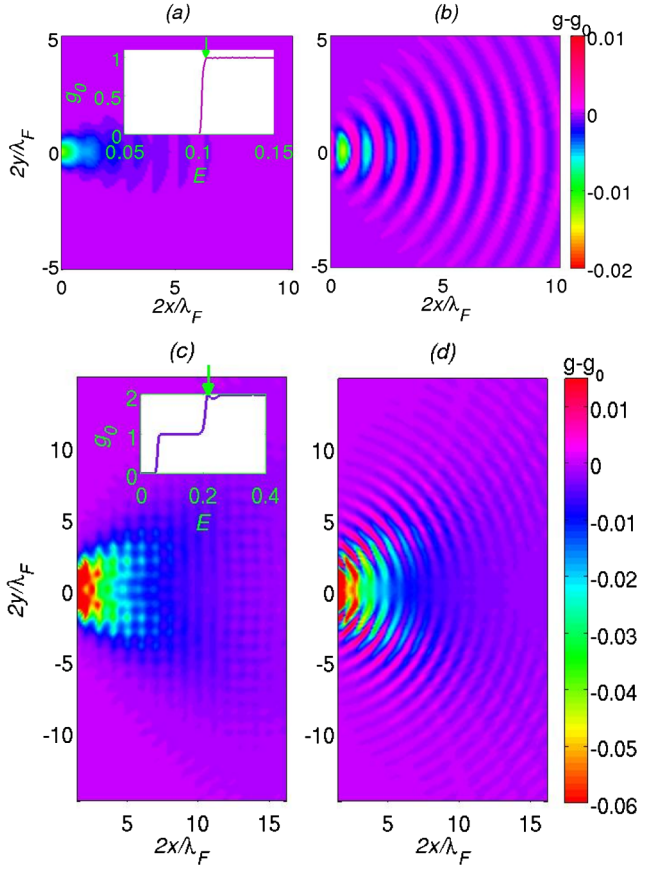

FIG. 2 (color online). $\delta g(T) = g(T) - g_0(T)$ as a function of the tip position (in units of $\lambda_F/2$). The left figures correspond to $T = 0$, while $T \neq 0$ for the right figures. g_0 is biased as indicated by the arrow in the insets [giving $g_0(T = 0)$ as a function of E_F]. (a),(b): QPC opened at the beginning of the first plateau using model 1 with $V = 1$ and $\lambda_F/2 = 9.65$. $k_B T/E_F = 0.01$ for (b) $(2l_T/\lambda_F \approx 14.6)$. (c),(d): QPC opened at the beginning of the second plateau using model 2 with $V = -2$ and $\lambda_F/2 = 6.7$. $k_B T/E_F = 0.035$ for (c) $(2l_T/\lambda_F \approx 4)$.

$g_0 = 1$ only at resonance. Nevertheless, we expect that the fast energy dependence of g_0 in the RLM model can be used for describing the sharp *opening* of the first QPC conduction channel. Let us first study the limit $T = 0$. Without the tip, $g_0(E)$ [in units of $2(e^2/h)$] can be expressed [16] in terms of the self-energies $\Sigma_{l,r}(E) = R_{l,r}(E) + iI_{l,r}(E)$ of the left l and right r leads:

$$g_0(E) = \frac{4I_l I_r}{(E - V_{\mathbf{0}} - R_l - R_r)^2 + (I_r + I_l)^2}. \quad (1)$$

$\Sigma_{l,r}(E)$ are related to the retarded Green's functions of the 2 leads evaluated at the 2 sites directly coupled to $\mathbf{0}$: $\Sigma_{l,r}(E) = t_c^2\langle \pm 1, 0|G^R_{l,r}(E)| \pm 1, 0\rangle$. If t_c is small, the transmission exhibits a sharp Breit-Wigner resonance of width $\Gamma = -(I_l + I_r)$ at an energy $V_{\mathbf{0}} + R_l + R_r$. The Green's function of semi-infinite square lattices can be obtained from the expression valid for an infinite square lattice using the method of mirror images [17].

In the presence of the tip, the conductance $g(E)$ of the QPC-tip interferometer is still given by Eq. (1), if one adds to the self-energy $\Sigma_r(E)$ of the right lead an amount $\Delta\Sigma_r(E)$ which accounts for the effect of the tip. This generalization of formula (1) uses a method introduced in Ref. [18] and will be given in a following paper [19]. From Dyson's equation, one gets $\Delta\Sigma_r(E) = t_c^2\rho\exp(i\phi)|\langle 1, 0|G^R_r|x, 0\rangle|^2$, where ρ and ϕ are, respectively, the modulus and the argument of the scattering amplitude $V/(1 - V\langle x, 0|G^R_r|x, 0\rangle)$. Neglecting the x dependences of ρ and ϕ at large distance, one gets in the continuum limit

$$\frac{\Delta\Sigma_r(E)}{t_c^2} \approx -\frac{\rho k \exp[i(2kx + \pi/2 + \phi)]}{2\pi x} + O\left(\frac{1}{x^{3/2}}\right). \quad (2)$$

Since $\Delta\Sigma_r(E) \to 0$ as x increases, the effect $\delta g = g - g_0$ of the tip upon g_0 can be expanded in powers of the reduced variables $\delta R = \Delta R/I$ and $\delta I = \Delta I/I$ (with $I = I_{r,l} \approx -t_c^2k^2/4$ and $\Delta\Sigma_r = \Delta R + i\Delta I$). The coefficients depend on g_0 and on $S_0 = g_0(1 - g_0)$:

$$\delta g = sg_0\sqrt{S_0}\delta R + S_0\delta I + sg_0\sqrt{S_0}(1 - 2g_0)\delta R\delta I + g_0^2(\tfrac{3}{4} - g_0)\delta R^2 + g_0^2(-\tfrac{5}{4} + g_0)\delta I^2, \quad (3)$$

where $s = \mathrm{sgn}[(E - V_{\mathbf{0}} - 2R)/2I]$.

Out of resonance ($g_0 < 1$), the linear terms give fringes of period $\lambda_F/2$ falling off as $1/x$:

$$\frac{\delta g}{g_0} \underset{g_0<1}{\approx} \frac{2\rho\sin\zeta_0\cos(2k_Fx + \theta)}{\pi k_F x} + O\left(\frac{1}{x^{3/2}}\right), \quad (4)$$

where $\theta \equiv \pi/2 + \phi - \zeta_0$ with $\sin\zeta_0 \equiv s\sqrt{1 - g_0}$. At resonance ($g_0 = 1$), the linear terms vanish and the quadratic terms give a nonoscillatory negative correction which falls off as $1/x^2$ accompanied by fringes δg_{osc} with period $\lambda_F/2$ and $1/x^{5/2}$ decay:

$$\frac{\delta g}{g_0} \underset{g_0=1}{\approx} -\left(\frac{\rho}{\pi k_F x}\right)^2 - \delta g_{\mathrm{osc}}. \quad (5)$$

These two behaviors of δg characterizing the RLM model (at or out of resonance) have the same origin than those obtained in Ref. [11] for a QPC (inside or outside a plateau).

Let us study the TIFs occurring in the RLM model when E_F is located on the transmission peak ($g_0 = 1$ when $T = 0$). The quantum statistics give an energy scale $\approx k_BT$. The resonant contact gives another energy scale, since it restricts the transmission inside an energy window Γ around E_F. This gives two length scales (over which an electron propagates at the Fermi velocity during the associated time scales) the thermal length $l_T = k_F/(4k_BT\pi^{-1/2})$ yielded by the quantum statistics and the length $l_\Gamma = k_F/\Gamma$ yielded by the resonance. The temperature dependence of the TIFs is a function of these two scales. The effect of the tip $\delta g(T)$ at a temperature T is given by $\int \delta g(E) \times [-\partial f_T(E)/\partial E]dE$, where $\delta g(E)$ is given by Eq. (3) and $f_T(E)$ is the Fermi distribution at an energy E (one has $-4k_BT\partial f_T(E)/\partial E \approx \exp-[(E - E_F)/(4k_BT\pi^{-1/2})]^2$). If E_F is at resonance, $\delta g(x)$ shows only weak oscillations at $T = 0$ [Eq. (5)]. When $T \neq 0$, $S_0(E) \neq 0$ for electrons of energies E around E_F, yielding TIFs via their linear ρ/x contributions in the expansion (3). Doing standard approximations (see Ref. [20]), we get for these TIFs

$$\frac{\delta g(T)}{g_0(T)} \approx A\left(\frac{x}{l_\Gamma}, \frac{l_T}{l_\Gamma}\right)\frac{\rho\cos(2k_Fx + \phi)}{2\pi k_F x} - \frac{\rho^2}{(\pi k_F x)^2}. \quad (6)$$

The amplitude A [shown in Fig. 3(b)] is given by

$$A(\mu, \nu) = \frac{(1 + 2\mu + 4\nu^2)F_+ + F_- - G}{\mathrm{erfc}(\nu)}, \quad (7)$$

where $F_\pm = e^{\pm\mu}\mathrm{erfc}[\frac{2\nu^2 \pm \mu}{2\nu}]$ and $G = (4\nu/\sqrt{\pi}) \times e^{-\nu^2-(\mu^2/4\nu^2)}$. Three main results can be seen: (i) A vanishes when $T \to 0$, i.e., when $l_T \gg l_\Gamma$. In the opposite regime, $l_T \ll l_\Gamma$, (ii) when $x \gg l_T$, there is a universal asymptotic $\exp(-x/l_\Gamma)$ decay characterized by the T-independent scale l_Γ and not by l_T; (iii) A has a maximum when $x \approx l_T$. In Fig. 3(a), one can check that the analytical behaviors [Eq. (6)] reproduce the results of numerical simulations. So far, we have described the TIFs at resonance. Studying the fringes outside the resonance [$g_0(E_F) \neq 1$], it can be shown [19] that their amplitude A remains a function of x/l_Γ and l_T/l_Γ. Since A becomes negligible as $T \to 0$ only when $g_0 \approx 1$ [see Eq. (4)], one finds that the thermal enhancement of the fringes persists only in an energy window $\approx 0.2\Gamma$ around the resonance.

These results obtained with the RLM model can be extended to a QPC with $g_0 \leq 1$. We have checked [19] that the expansion (3) describes also (up to a phase factor) the effect of a tip upon a QPC when $g_0 \leq 1$, if one uses in Eq. (3) the steplike function $g_0(E)$ of the QPC instead of

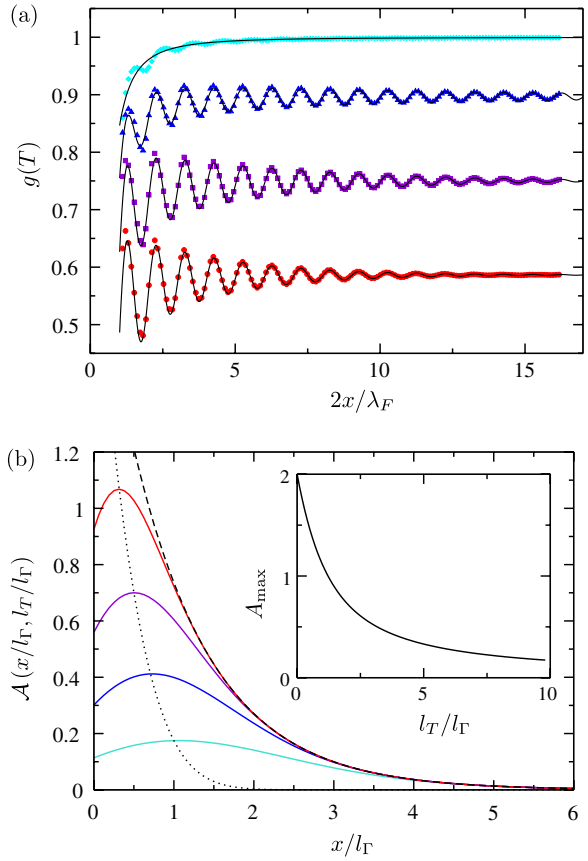

FIG. 3 (color online). (a) RLM conductance $g(T)$ as a function of $2x/\lambda_F$ for increasing temperatures (from top to bottom). The color points are results obtained by direct numerical simulations, taking from top to bottom $2l_T/\lambda_F = \infty$, 8.8, 4.4, and 2.2. The solid lines give the analytical results [Eq. (6)]. $t_c = 0.4$, $V = -2$, $\lambda_F/2 \approx 10$, and $2l_\Gamma/\lambda_F \approx 4$. (b) As a function of x/l_Γ, rescaled amplitude $\mathcal{A} = A(x/l_\Gamma, l_T/l_\Gamma)\mathrm{erfc}(l_T/l_\Gamma)$ for fixed l_Γ and increasing temperatures, i.e., ratios $l_T/l_\Gamma = 1$ (light blue), 0.7 (blue), 0.5 (violet), and 0.3 (red) (solid lines from bottom to top). The dashed and dotted lines give, respectively, the asymptotic behavior $2\exp(-x/l_\Gamma)$ valid for $x \gg l_T$ and the function $\mathcal{A}(l_T/l_\Gamma, l_T/l_\Gamma)$, where $\mathcal{A}$ is maximum. Inset: Maximum $A_{\max}$ of the bare amplitude A as a function of l_T/l_Γ.

the Lorentzian $g_0(E)$ of the RLM model. Since the linear terms in Eq. (3) depend on $g_0(E)$ through the combination $S_0(E) = g_0(E)[1 - g_0(E)]$, the scale Γ for a QPC is given by the energy window where $S_0(E) \neq 0$, i.e., by the change of Fermi energy required to open a new QPC channel at $T = 0$. As for the RLM model, Γ gives also the energy window (location of the arrows in the insets in Fig. 2) for observing TIFs at the edges of the plateaus.

In summary, temperature-induced fringes can be observed in the SGM images of a QPC biased near the ends of conductance plateaus. These fringes vanish when $T \to 0$, depend on the ratio l_T/l_Γ, and decay with a T-independent length l_Γ. The sharper the contact opening, the smaller the energy Γ, and the larger the length l_Γ where these fringes can be observed beyond l_T. We predict that very visible TIFs should be observed in a small energy window of order Γ for E_F in long adiabatic contacts opened at the edges of the $T = 0$ conductance plateaus.

We thank A. Freyn, R. A. Jalabert, K. A. Muttalib, F. Portier, and D. Weinmann for useful discussions and the French National Agency ANR (Project No. ANR-08-BLAN-0030-02 "Item-Th") for financial support.

[1] B. J. van Wees *et al.*, Phys. Rev. Lett. **60**, 848 (1988).
[2] D. Wharam *et al.*, J. Phys. C **21**, L209 (1988).
[3] L. Glazman, G. Lesovik, D. Kmelnitskii, and R. Shekhter, JETP Lett. **48**, 238 (1988).
[4] M. Büttiker, Phys. Rev. B **41**, 7906 (1990).
[5] C. W. J. Beenakker and H. Van Houten, Solid State Phys. **44**, 1 (1991).
[6] K. J. Thomas *et al.*, Phys. Rev. Lett. **77**, 135 (1996).
[7] M. Topinka, B. LeRoy, S. Shaw, E. Heller, R. Westervelt, K. Maranowski, and A. Gossard, Science **289**, 2323 (2000).
[8] M. Topinka, B. LeRoy, R. Westervelt, S. Shaw, R. Fleischmann, E. Heller, K. Maranowski, and A. Gossard, Nature (London) **410**, 183 (2001).
[9] M. Topinka, R. Westervelt, and E. Heller, Phys. Today **56**, No. 12, 47 (2003).
[10] B. J. LeRoy *et al.*, Phys. Rev. Lett. **94**, 126801 (2005).
[11] R. A. Jalabert, W. Szewc, S. Tomsovic, and D. Weinmann, Phys. Rev. Lett. **105**, 166802 (2010).
[12] M. P. Jura, M. A. Topinka, M. Grobis, L. N. Pfeiffer, K. W. West, and D. Goldhaber-Gordon, Phys. Rev. B **80**, 041303 (2009).
[13] E. Heller, K. Aidala, B. LeRoy, A. Bleszynski, A. Kalben, R. Westervelt, K. Maranowski, and A. Gossard, Nano Lett. **5**, 1285 (2005).
[14] M. P. Jura *et al.*, Nature Phys. **3**, 841 (2007).
[15] A. Freyn, I. Kleftogiannis, and J.-L. Pichard, Phys. Rev. Lett. **100**, 226802 (2008).
[16] S. Datta, *Electronic Transport in Mesoscopic Systems* (Cambridge University Press, Cambridge, England, 1997).
[17] M. I. Molina, Phys. Rev. B **74**, 045412 (2006).
[18] P. Darancet, V. Olevano, and D. Mayou, Phys. Rev. B **81**, 155422 (2010).
[19] G. Lemarié, A. Abbout, and J.-L. Pichard (to be published).
[20] F. Mezei and G. Grüner, Phys. Rev. Lett. **29**, 1465 (1972).